American Mineralogist, Volume 79, pages 892–903, 1994

Differential incorporation of trace elements and dissymmetrization in apatite: The role of surface structure during growth

JOHN RAKOVAN, RICHARD J. REEDER

Department of Earth and Space Sciences, State University of New York at Stony Brook, Stony Brook, New York 11794-2100, U.S.A.

ABSTRACT

Apatite crystals from Llallagua, Bolivia, and Minas Gerais, Brazil, show heterogeneous distributions of trace elements that correspond directly to coeval portions of symmetrically nonequivalent vicinal faces of growth hillocks on both $\{10\bar{1}0\}$ and $\{0001\}$ faces (i.e., intrasectoral zoning). The same samples also exhibit sectoral zoning. Synchrotron X-ray fluorescence microanalysis (SXRFMA) reveals differences up to a factor of 2 in Y and 1.5 in Sr concentrations between subsectors associated with symmetrically nonequivalent vicinal faces of trigonal growth hillocks on $\{10\bar{1}0\}$ faces. Trace amounts of REE and Mn show differential distribution patterns similar to those of Y and Sr. SXRFMA line scans and cathodoluminescence imaging indicate that the compositional differences are sharp and conform to face symmetry.

No variations are found in trace element concentrations between symmetrically equivalent pyramidal vicinal faces of hexagonal growth hillocks on $\{0001\}$ faces, also consistent with face symmetry. However, variations exist between these pyramidal vicinal faces and surfaces parallel to $\{0001\}$, which are found at the summits of many of these hillocks. Such variations indicate nonequilibrium partitioning and suggest that there is no unique value of K_D that describes the actual partitioning for a given mineral-fluid system; rather, effective K_D values differ for structurally distinct regions of a crystal surface.

Apatite samples from Llallagua also show optical anomalies that correspond directly to time-equivalent portions of different sectors and subsectors within single crystals. Sectors under $\{0001\}$ are uniaxial negative, whereas sectors under $\{10\bar{1}1\}$, $\{11\bar{2}1\}$, and $\{10\bar{1}0\}$ are biaxial. Subsectors associated with different vicinal faces within these individual sectors range in $2V$ from 2 to 15°. Surface structure not only plays an important role in the differential partitioning of trace elements into apatite during growth but also influences the ordering of atoms, leading to dissymmetrization.

INTRODUCTION

There is a large body of literature that investigates the many complex variables that affect the partitioning of trace elements into minerals during their formation. Trace element charge and size (Goldschmidt, 1937), electronegativity (Ringwood, 1955), crystal field effects (Burns, 1970), and crystal growth rate (Burton et al., 1953), as well as state variables such as temperature, pressure, and composition, have all been identified and studied as factors affecting trace element partitioning. More recently, several authors have demonstrated the role of surface structure on the partitioning of elements into crystals (Nakamura, 1973; Dowty, 1976b, 1977; Reeder and Grams, 1987; Paquette and Reeder, 1990). They have interpreted the differential incorporation of trace elements onto crystal surfaces during growth, leading to sectoral zoning, to be controlled by surface structure. Paquette and Reeder (1990) have identified surface structural control as the cause of intrasectoral zoning in calcite. Intrasectoral zoning describes compositional differences between time-equivalent portions of a given sector of a single crystal.

Here, we document the first example of intrasectoral zoning found in apatite (see also Rakovan and Reeder, 1992, 1993), further demonstrating the wide sphere of occurrences of this phenomenon. The presence of sectoral and intrasectoral zoning exemplifies the role of surface structure on the incorporation of trace elements into apatite during growth. Moreover, surface-controlled partitioning provides an explanation for the existence of heterogeneous element distributions, which are increasingly important in petrologic studies since these zoning types indicate nonequilibrium trace element partitioning. Although many studies have shown the importance of surface structure on trace element incorporation, few have proposed details on the mechanisms of surface structure influence (protosite configurations, etc.).

Apatite, $Ca_5(PO_4)_3(F,OH,Cl)$, is a ubiquitous accessory mineral in igneous rocks, and its presence can strongly influence the trace element evolution of magmas. It is also commonly found in low-temperature sedimentary

0003–004X/94/0910–0892$02.00

environments and as a precipitate from mesothermal and hydrothermal aqueous solutions. Many studies have shown apatite to be one of the most important minerals affecting rare earth element (REE) trends in igneous rocks (e.g., Nash, 1972; Bergman, 1979; Watson and Capobianco, 1981; Kovalenko et al., 1982; Gromet and Silver, 1983; Watson and Harrison, 1984a, 1984b). Thus, apatite chemistry can play a critical role in the understanding and modeling of igneous petrogenetic processes.

Because of its structure and composition, apatite lends itself to many compositional substitutions (McConnell, 1973). Si, As, and V can readily substitute for $^{[4]}P$. There are also two distinct Ca sites in the apatite structure. The Ca1 site is coordinated by nine O atoms, and the Ca2 site is coordinated by six O atoms and one of the column anions (F, Cl, or OH). The size and geometry of the Ca2 site vary, depending on the column anion. For a detailed description of the apatite structure and ternary variations thereof, see Hughes et al. (1989, 1990). Many substitutions for Ca exist, including K, Na, Mn, Ni, Cu, Co, Zn, Sr, Ba, Pb, Cd, Sn, Y, and REE. Substitution of trivalent cations such as REE for Ca^{2+} has been shown to be coupled with substitutions of Na^{+} for Ca^{2+} and Si^{4+} for P^{5+} to achieve charge balance (Ronsbo, 1989; Hughes et al., 1991b). Ronsbo (1989) showed in a suite of igneous rocks that the favored coupled substitution is dependent on both the alkalinity and silica activity of the liquid from which it crystallizes. Substitution of these elements commonly leads to a partially ordered arrangement within the Ca sites or the tetrahedral site in apatite (Hughes and Drexler, 1991; Hughes et al., 1991a, 1991b).

In this paper, we describe the occurrence of sectoral and intrasectoral zoning in apatite and discuss the implications for apatite geochemistry and for crystal growth in general. Mechanisms for differential incorporation of trace elements are also proposed.

Compositional zoning types in minerals

In this paper, compositional zoning differences are assumed to be of a substitutional, rather than interstitial, nature within a single crystal. Furthermore, we will only address zoning created during crystal growth. Several different types of compositional zoning are found in minerals, each of which provides unique information about the formation and growth history of a crystal. The most familiar kind of compositional zoning is concentric zoning, in which the contact between two portions of a crystal with different compositions is parallel to the growth surface. Thus this zoning type records the morphologic history of a crystal during growth. Concentric zoning most commonly reflects changes in the environment of growth over time (e.g., changes in chemical composition, temperature, supersaturation, etc.). If one assumes that growth occurs on the entire surface of a crystal (i.e., on all crystal faces), any given concentric zone comprises synchronous portions of all the sectors contained therein (Fig. 1). Hence, upon termination of growth, the last concentric zone to form is bounded by the crystal surface itself, and the different regions of that layer are coeval, or synchronous.

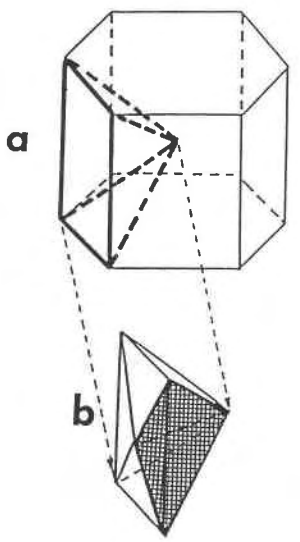

Fig. 1. (**a**) Schematic diagram of a hexagonal crystal with one of the $\{10\bar{1}0\}$ prism sectors outlined in bold dashed lines. (**b**) The sector isolated from the crystal. A four-sided growth hillock has been drawn on the prism face, and one of the subsectors is shaded.

Another kind of zoning found in minerals yields information about growth mechanism and the subtleties of element incorporation during growth. Two variations of this type can be identified: sectoral and intrasectoral zoning. Sectoral zoning is represented by compositional differences between time-equivalent portions of different sectors. Compositional interfaces for sectoral zoning correlate with growth sector boundaries, which, if present, cut across concentric zoning. Such compositional differences can only arise during the growth of a crystal, and correlation of compositional differences with different crystal faces suggests that the characteristics of the crystal surface lead to its formation (Dowty, 1976b; Reeder and Grams, 1987).

A compositional difference between time-equivalent portions of different subsectors is known as intrasectoral zoning (Paquette and Reeder, 1990). We define subsectors as regions within a given sector of a single crystal that have grown by the incorporation of growth units onto a given vicinal face of a polygonized growth hillock (Fig. 1). If growth on a crystal face occurs by the spiral mechanism, hillocks will generally develop on that face. Growth hillocks comprise very shallow, nonrational surfaces called vicinal faces. A vicinal face is a crystal face that modifies a normal crystal face, which it closely approximates in angle, and is composed of an array of growth steps having like orientation and advancing in the same direction during growth. Growth hillocks may be polygonized, with straight step segments meeting at well-defined angles, or they may be rounded.

Intrasectoral zoning provides unique information about

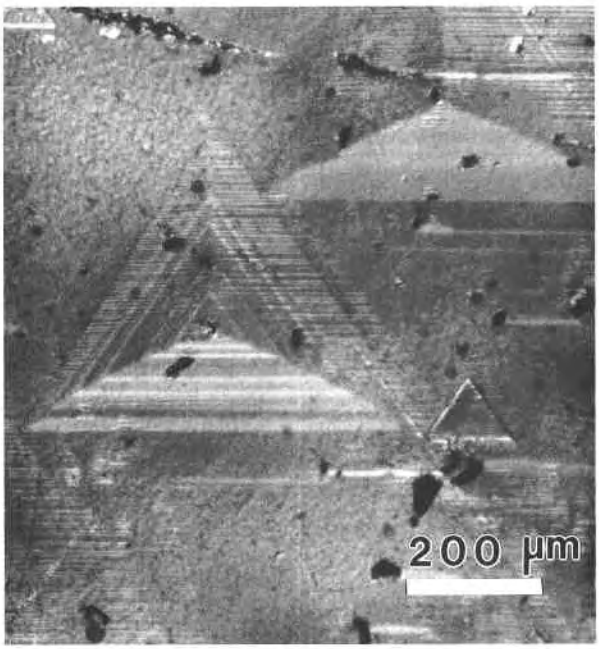

Fig. 2. DIC photomicrograph of a $\{10\bar{1}0\}$ face on Golconda apatite, showing a trigonal growth hillock. The three vicinal faces of the hillock exhibit macrosteps. The scale bar is parallel to [0001]. Faint striations parallel to [0001] are etch features.

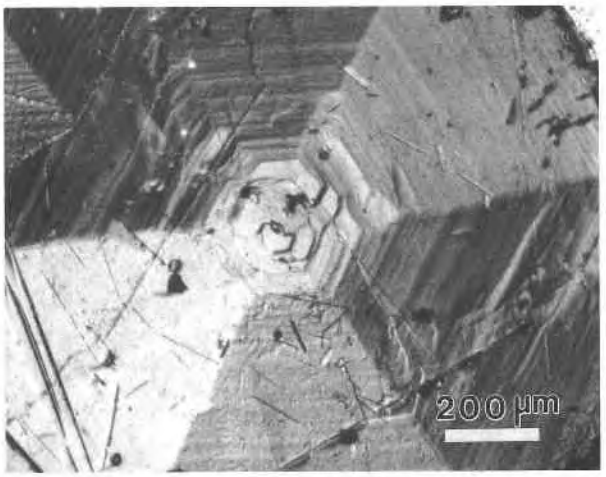

Fig. 3. DIC photomicrograph of a {0001} face on the Llallagua-2 apatite, showing a hexagonal growth hillock. The six pyramidal vicinal faces of the hillock exhibit macrosteps. A six-fold axis of rotation perpendicular to {0001} symmetrically equates the six vicinal faces.

the crystal growth process. The compositional interface correlates with subsector boundaries and crosscuts any existing concentric zoning. Because of its nature, intrasectoral zoning indicates growth of a sector by the spiral mechanism.

Samples

Two suites of apatite crystals were used in this study. The first group of samples is from the Golconda mine, Minas Gerais, Brazil. They were found in a late-stage pocket assemblage in the Golconda pegmatite and most likely formed from pegmatitic hydrothermal fluids. The Golconda is a tourmaline-rich, REE-rich, granitic pegmatite (Proctor, 1985). Apatite crystals are doubly terminated and euhedral. They are elongate along **c**, have an average aspect ratio of 6, and are dominated by $\{10\bar{1}0\}$. Individual crystals range from 3 mm to >2 cm in length. The crystal faces are very lustrous for the most part, and surface growth features (i.e., growth hillocks) have been well preserved. Samples are transparent, with a very light pink color.

The second suite of samples (Los Angeles Museum of Natural History no. 35673) is from the 295th level of the Contacto vein, Llallagua, Bolivia. They were found as late-stage pocket minerals (Kampf, 1982) in hydrothermal Sn-W veins. Crystals are euhedral and tabular, with an average aspect ratio of 0.15, and range from 0.5 to 2.0 cm in diameter. Forms present are $\{10\bar{1}1\}$, $\{10\bar{1}0\}$, $\{11\bar{2}1\}$, $\{11\bar{2}0\}$, and {0001}, with {0001} dominant. The hexagonal dipyramid faces are preferentially etched, whereas the basal pinacoid and prism faces retain growth features. Samples are colorless and transparent. One crystal of Llallagua apatite (American Museum no. 32870) that was studied did not come from the same location in the mine as the other samples. It is also tabular but exhibits only $\{10\bar{1}0\}$ and {0001}. This specimen is referred to here as Llallagua-2.

Surface microtopography and growth features were imaged using differential interference contrast (DIC) microscopy. The $\{10\bar{1}0\}$ faces on the Golconda apatite samples and the Llallagua-2 apatite exhibit well-formed trigonal growth hillocks (Fig. 2). Macrosteps are visible on the three vicinal faces of many of these hillocks.

The {0001} faces on all of the Llallagua apatite samples show well-developed hexagonal growth hillocks that are composed of six pyramidal vicinal faces (Fig. 3). On the Llallagua-2 crystal, these hillocks have macrosteps that are preserved on their vicinal faces. The other Llallagua apatite samples have been slightly etched, and no macrosteps are preserved. The hillocks on these samples are also truncated by a flat surface parallel to {0001}.

Analytical techniques

Qualitative and quantitative compositional analyses of regions within individual sectors and subsectors were conducted using cathodoluminescence microscopy (CL), electron microprobe analysis (EMPA), and synchrotron X-ray fluorescence microanalysis (SXRFMA).

Major element chemistries were determined using a Cameca Camebax electron probe operating at 15 kV and 15–20 nA; ten replicate analyses were averaged for each spot analyzed. To minimize the effect of column anion migration (Stormer et al., 1993), a spot size of 11 μm was

used with variable collection times on {10$\bar{1}$0} sections. The samples that were analyzed with EMPA had not been subjected previously to electron beam irradiation, using either CL or other techniques. Natural phosphate and carbonate standards were used to determine the abundances of Ca, P, Mn, and Sr. A synthetic Y phosphate standard was used to determine O, and an apatite standard from Durango, Mexico, was used for F. Because of the problems encountered in EMPA of apatite (Stormer et al., 1993), the F analysis is suspect. Crystals were cut in half and analyzed along transects from the core to the rim. EMPA shows that the Golconda samples are end-member fluorapatite, $Ca_5(PO_4)_3F$. The Llallagua apatite samples are binary hydroxylapatite-fluorapatite, $Ca_5(PO_4)_3(F_{0.8}OH_{0.2})$.

CL images of crystal growth surfaces were used as qualitative maps of the distribution of CL-activating or quenching trace elements. The images were collected on a cold-cathode Technosyn CL stage operating between 10–15 keV and 500–600 μA.

Trace element abundances and spatial distributions were quantitatively determined by SXRFMA at the X26A beam line at the National Synchrotron Light Source (NSLS) at Brookhaven National Laboratory, Upton, New York. Correlation of compositional differences with crystal surface features was accomplished by the analysis of oriented thin sections. Typically, a growth face of the crystal was cemented to a glass slide, and the section was prepared using standard thin-section techniques. The sample was then transferred from the original slide to another, with the crystal face oriented up. This procedure produced samples comprising the 20–60 μm of a crystal closest to the surface within a given sector. During the analysis of such samples, the fluorescence signal was derived from within this outermost 20–60 μm of the crystal; hence, all analyses therein are essentially from time-synchronous portions of the crystal.

Several considerations must be observed in thin section preparation for SXRFMA. The backing material must be free of detectable amounts of any element of interest in the experiment. Ultrapure silica glass (Suprasil made by Heraus Amersil) was used for slides. The mounting glue must also be free of such impurities. Epotek 301 epoxy or Krazy Glue (cyanoacrylate) was used in all experiments.

Data were collected using a white synchrotron beam collimated to an incident size between 8 and 10 μm. The effective energy range of excitation for the X26A beam line at NSLS is 3–30 keV. *K* lines were used for elements up to Sn, and *L* lines were used for all heavier elements. The intense fluorescence signal of Ca was reduced by placing a Kapton filter (488 μm thick) in the reflected beam path. A portion of the reflected beam path (1–5 cm) is through air; hence, signals from elements lighter than Ca were strongly attenuated.

A Li-drifted Si energy-dispersive spectrometer (EDS) was used for data collection. EDS resolution is approximately 160 eV at 5.895 keV. Detection limits with a 10-μm white beam range from 0.1 to 10 ppm, depending on the element and the matrix analyzed (Jones and Gorden, 1989). Several modes of data collection are possible: individual spot analyses, one-dimensional line scans, and two-dimensional area scans. Spot analyses were collected using a live time of 5 min. The total number of counts, and hence statistical precision, for any given analysis time is dependent on the atomic weight and concentration of the element in question. Line and area scans were conducted with variable numbers of analyses and count times. Scan data were collected as regions of interest over a defined energy range.

EDS spectra were fitted to obtain accurate fluorescence peak intensities. The elemental concentrations were obtained using a so-called standardless analysis, in which the concentration of one of the detected elements, in this case Ca, is known from EMPA, and relative proportions of other elements were calculated. Calculations were carried out using a modified version of the Naval Research Laboratory program NRLXRF (Criss, 1977). ZAF effects as well as sample thickness, incident and reflected beam absorption by air and filters, and experimental geometry are accounted for in this program.

Standard optical microscopy was used to determine the optical character of the apatite samples. Oriented sections were cut from the interior of single crystals so as to contain either the {0001} sector only or the {10$\bar{1}$1}, {11$\bar{2}$1}, and {10$\bar{1}$0} sectors.

Results

Surface growth features

{10$\bar{1}$0}. DIC imaging of the surface microtopography shows well-developed growth hillocks on {10$\bar{1}$0} and {0001} faces (Figs. 2 and 3), indicating growth on these forms by the spiral mechanism. Trigonal growth hillocks on the {10$\bar{1}$0} faces of both the Golconda apatite samples and the Llallagua-2 apatite are approximately symmetric, with equal development of the three vicinal faces (Fig. 2). The face symmetry of {10$\bar{1}$0} is a mirror plane perpendicular to [0001]. The orientation of the trigonal hillocks on these faces is such that two of the vicinal faces are symmetrically related by the mirror, shown schematically in Figure 4. The third, or basal, vicinal face, whose growth steps are parallel to [0001], is not related to the others by any symmetry element (Fig. 4). Typically, there are between 10 and 30 hillocks on any given prism face of the Golconda samples, with flat regions in between. The hillocks have an average edge length of approximately 400 μm. Only a few (1–4) are present on each prism face on the Llallagua-2 sample. The larger part of the Llallagua-2 prisms are heavily striated, as is typical of most single crystals of apatite. The striations are parallel to [0001] and are also parallel to growth steps making up the basal vicinal face. Striations on this particular sample are most likely due to preferential growth of [0001] steps on the nonequivalent vicinal face.

{0001}. Hexagonal growth hillocks on the {0001} faces of the Llallagua apatite samples are also symmetric, with

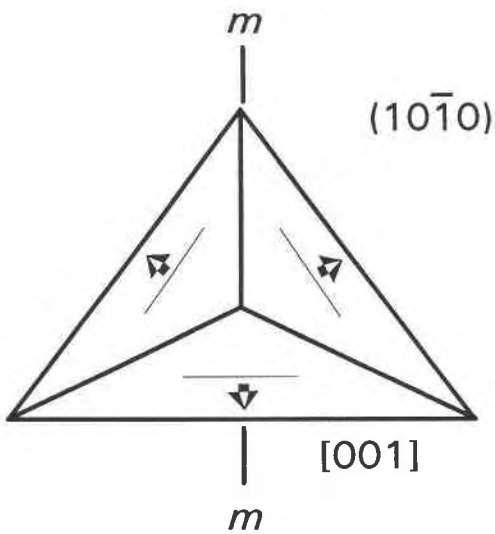

Fig. 4. Schematic diagram of a trigonal growth hillock on the apatite {10$\bar{1}$0}. The face symmetry has a mirror plane perpendicular to [0001], symmetrically equating the two upper vicinal faces. The third basal vicinal face is symmetrically nonequivalent. Lines within each vicinal face represent the orientations of growth steps. Arrows indicate the directions of advancement of these steps during growth. Steps on the basal vicinal face are parallel to [0001].

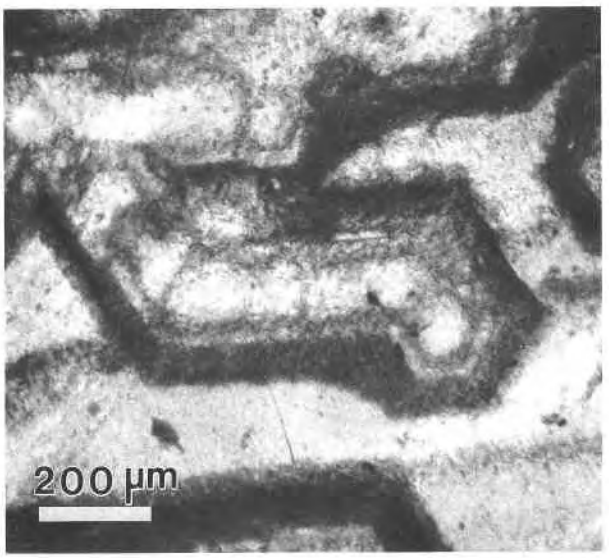

Fig. 5. DIC photomicrograph of a {0001} face on Llallagua apatite, showing kinked plateaus formed by the coalescence of multiple hexagonal growth hillocks.

equal development of the six pyramidal vicinal faces. These hillocks are made up of growth steps parallel to ⟨11$\bar{2}$0⟩. The face symmetry of {0001} is a sixfold axis of rotation. This axis symmetrically equates all six pyramidal vicinal faces. Most of the {0001} hillocks on the Llallagua-2 crystal comprise the six pyramidal vicinal faces only. However, some have developed {0001} surfaces at their summit. These surfaces apparently formed by the termination of growth parallel to ⟨001⟩ while growth steps continued to spread laterally. The density of hillocks on {0001} of the Llallagua-2 apatite is very high, covering the entire surface. The average edge length of these hillocks is 800 μm.

Hexagonal growth hillocks on {0001} faces of the other Llallagua apatite samples all exhibit the basal surface at their apexes. No steps have been preserved on these hillocks. However, it is presumed that the basal surfaces formed by the same mechanisms as did those on the Llallagua-2 sample. Hillock density is also high on these crystals; however, there are flat regions of {0001} still present between hillocks. The average hillock size is 250 μm across. All hexagonal hillocks on the Llallagua-2 apatite are distinct. In comparison, many of the hillocks on the other Llallagua apatite samples have coalesced to form linear and kinked ridges with continuous pyramidal edges and a flat (0001) top (Fig. 5).

Cathodoluminescence

CL images of {10$\bar{1}$0} and {0001} crystal faces exhibit dramatic differences in luminescence that correlate exactly with symmetrically nonequivalent growth features. CL activation is not restricted to the crystal surface but involves activation from an estimated depth of 2–8 μm below the surface in nonmetallic minerals (Marshall, 1988). Hence, observed luminescence on a given vicinal face reflects the composition of the surface and a portion of the corresponding subsector.

The {10$\bar{1}$0} faces of the Golconda apatite crystals luminesce orange in subsectors under the two symmetrically equivalent vicinal faces of the trigonal growth hillocks (Fig. 6). Previous studies of CL in apatite have attributed orange luminescence to Sm and blue to Eu (Marshall, 1988). The orange luminescence is homogenous between the two vicinal faces on any hillock and between any two hillocks. Subsectors under the third nonequivalent vicinal face luminesce blue (Fig. 6). The contact between the orange and blue luminescence is sharp and corresponds directly to the boundary between nonequivalent vicinal faces. Such a differential luminescence suggests a differential distribution of activating or quenching trace elements between synchronous portions of different subsectors within a given sector—hence intrasectoral zoning.

The {10$\bar{1}$0} faces of the Llallagua-2 apatite also show differential luminescence that corresponds directly with the symmetrically nonequivalent vicinal faces on trigonal growth hillocks. These faces differ from those of the Golconda samples in that the two equivalent vicinal faces luminesce yellow, which we inferred was the result of Mn activation (Marshall, 1988), whereas the nonequivalent vicinal face luminesces a light blue.

CL of the six pyramidal vicinal faces of hillocks on the {0001} of Llallagua apatite crystals is homogenous, as expected from symmetry. Pyramidal vicinal faces luminesce an intense royal purple (Fig. 7). The {0001} faces

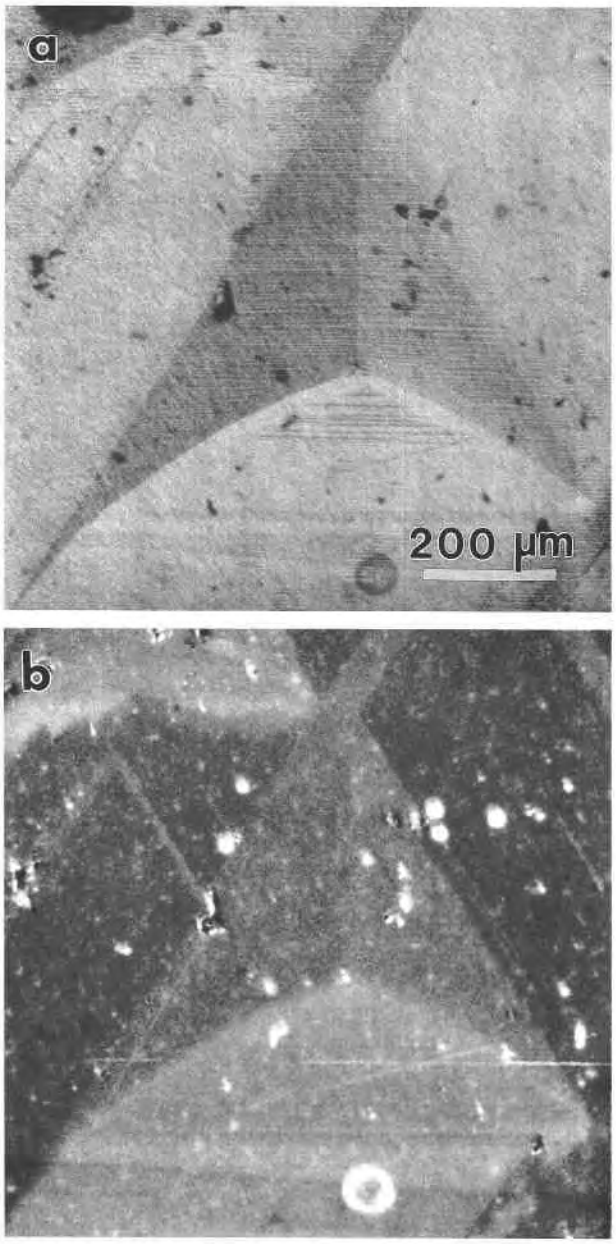

Fig. 6. (**a**) DIC photomicrograph of a trigonal growth hillock on the $\{10\bar{1}0\}$ of Golconda apatite. The mirror is vertical in this orientation. (**b**) Cathodoluminescence photomicrograph of the hillock in **a**. Luminescence is homogenous between the two symmetrically equivalent vicinal faces (luminescence color is orange). Differential luminescence exists between these and the nonequivalent vicinal face, whose luminescence is blue.

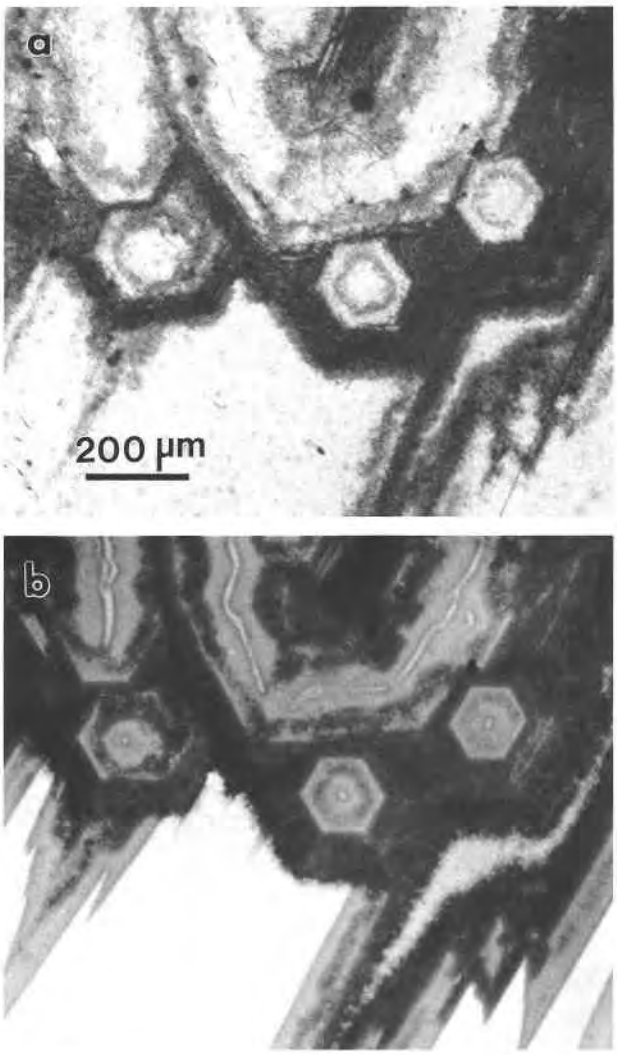

Fig. 7. (**a**) DIC photomicrograph of several hexagonal growth hillocks on the {0001} of Llallagua apatite. (**b**) Cathodoluminescence photomicrograph of the hillocks imaged in **a**. Luminescence is homogenous between the six symmetrically equivalent vicinal faces (luminescence color is purple). Differential luminescence exists between these and the surface parallel to {0001}, whose luminescence is lemon yellow.

of the Llallagua-2 apatite are almost entirely purple in CL, in stark contrast to the differential yellow and blue luminescence of the prism faces on this crystal, suggesting sectoral zoning. Small regions of yellow luminescence occur where some hillocks on this sample have developed a surface parallel to {0001}. All of the {0001} hillocks on the other Llallagua apatite samples have surfaces at their apex that are parallel to {0001}, and these also luminesce an intense yellow. Large flat regions of the {0001} surface where no hillocks are present luminesce a similar yellow color (Fig. 7).

Trace element chemistry

SXRFMA of individual vicinal faces and associated subsectors of $\{10\bar{1}0\}$ sectors reveals the presence of Mn, Sr, Y, and REE in trace amounts. The fluorescence peaks Sr$K\alpha$, Sr$K\beta$, Y$K\alpha$, and Y$K\beta$ are fully resolved. A representative SXRFMA spectrum is shown in Figure 8. Because of the resolution of the EDS detector and the small differences in energy among the REE L lines and the MnK lines, there is significant overlap of the fluorescence peaks

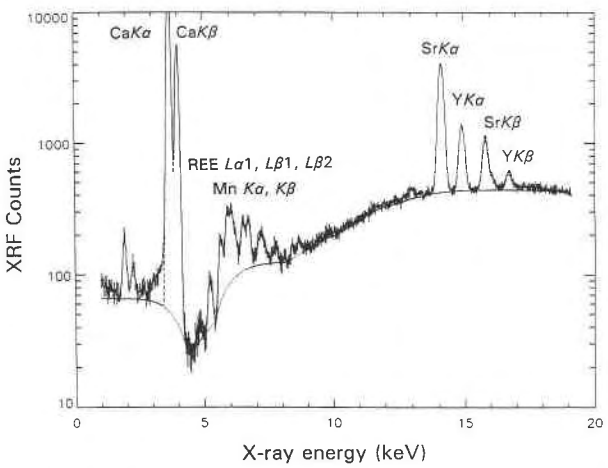

Fig. 8. Representative SXRFMA EDS spectrum of the Golconda apatite. Ca, Sr, and Y lines are well resolved. There is significant overlap of the REE and Mn peaks between 4.5 and 9 keV.

of these elements. Consequently, it was not possible to quantify differences in concentration of these elements.

Differences in the concentration of all the trace elements are found between symmetrically different subsectors of a given growth hillock. To correlate compositional differences with different growth features, line and area scans were taken over individual hillocks. Figure 9 shows the variation in Y concentration between two nonequivalent subsectors along transect a-b. A sharp twofold difference in Y concentration is seen; the compositional interface corresponds directly with the vicinal face boundary. Absolute concentrations of each trace element, determined from spot analyses at line scan end points a and b, are given in Table 1. Owing to the difficulty of accurately resolving the REE and Mn peaks, correlations are poorly defined for these elements, although variations are evident.

Similar results are shown for Y in an area scan of the small hillock in Figure 10. In this scan, higher elemental concentrations are plotted in lighter shades of gray and lower concentrations in gradationally darker shades. Again, differences in the concentration are sharp and correlate directly with the symmetrically nonequivalent vicinal faces of these hillocks. However, trace element concentrations are indistinguishable between the two equivalent vicinal faces. A similar distribution was observed in an area scan for Er, although increased noise is evident. No SXRFMA data are available from the Llallagua-2 apatite. The other Llallagua apatite samples contain trace amounts of Mn, Cu, Zn, As, Sr, Y, REE, and possibly U and Pb. As shown previously (Ronsbo, 1989; Hughes et al., 1991b), REE substitutions in apatite are commonly coupled with substitutions of Si and Na. Trace amounts of Si and Na were not detectable with the analytical methods used in this study. However, it is likely that the incorporation of these two elements is also affected by surface structure and that differential partitioning may occur. If the substitution of REE is coupled with that of Si and Na, the differential partitioning of REE may be affected by the degree of differential partitioning of Si and Na.

Table 1. Trace element concentrations in subsectors of Golconda apatite samples in Figs. 9 and 10

Sample	Point	Sr (ppm)	Y (ppm)
602a-2	*a*	360 ± 4	110 ± 1
602a-2	*b*	552 ± 6	200 ± 2
602c-1	1	140 ± 14	158 ± 16
602c-1	2	861 ± 9	300 ± 3

Note: because of the resolution of the EDS spectrometer, REE and Mn concentrations could not be quantitatively determined.

As expected from symmetry equivalence and as suggested by the CL observations, no variations in trace element concentrations exist between the six pyramidal vicinal faces of hexagonal {0001} hillocks. Line scans between pyramidal vicinal faces show no variation in trace element concentrations. Concentrations of the various trace elements, however, are different between subsectors under the pyramidal vicinal faces and the small {0001} surfaces that cap the hillocks.

Optical character

An important related feature of the Llallagua apatite samples that is not found in the Golconda samples is optically anomalous regions that correspond directly with different sectors and subsectors. The {0001} sectors are uniaxial negative, as would be expected for $P6_3/m$ apatite. However, $\{10\bar{1}1\}$, $\{11\bar{2}1\}$, and $\{10\bar{1}0\}$ sectors show biaxial character, indicating a lower symmetry in these sectors. Biaxial sectors also show distinct concentric zoning, with different concentric zones varying in both extinction orientation and $2V$. Polygonized and optically distinct subsectors that cut across concentric zones are noted within individual sectors. Time-equivalent portions of a given sector, as indicated by a single continuous concentric zone, show differences in $2V$ from 2 to as much as 15°.

Discussion

The spatially resolved compositional differences described within $\{10\bar{1}0\}$ and {0001} faces and their corresponding sectors represent intrasectoral zoning. Qualitative indication of intrasectoral zoning is given by CL of crystal faces in the samples studied. The differential distribution of CL colors (Figs. 6 and 7) indicates a corresponding differential distribution of activating or quenching trace elements. CL differences on $\{10\bar{1}0\}$ and {0001} faces of the Llallagua apatite samples correspond exactly with symmetrically nonequivalent vicinal faces of growth hillocks. Because the presence of hillocks is indicative of spiral growth, the direct correlation of different CL with different vicinal faces on a hillock indicates that intrasectoral zoning must have formed during growth and not as a result of postgrowth processes. Moreover, the changes

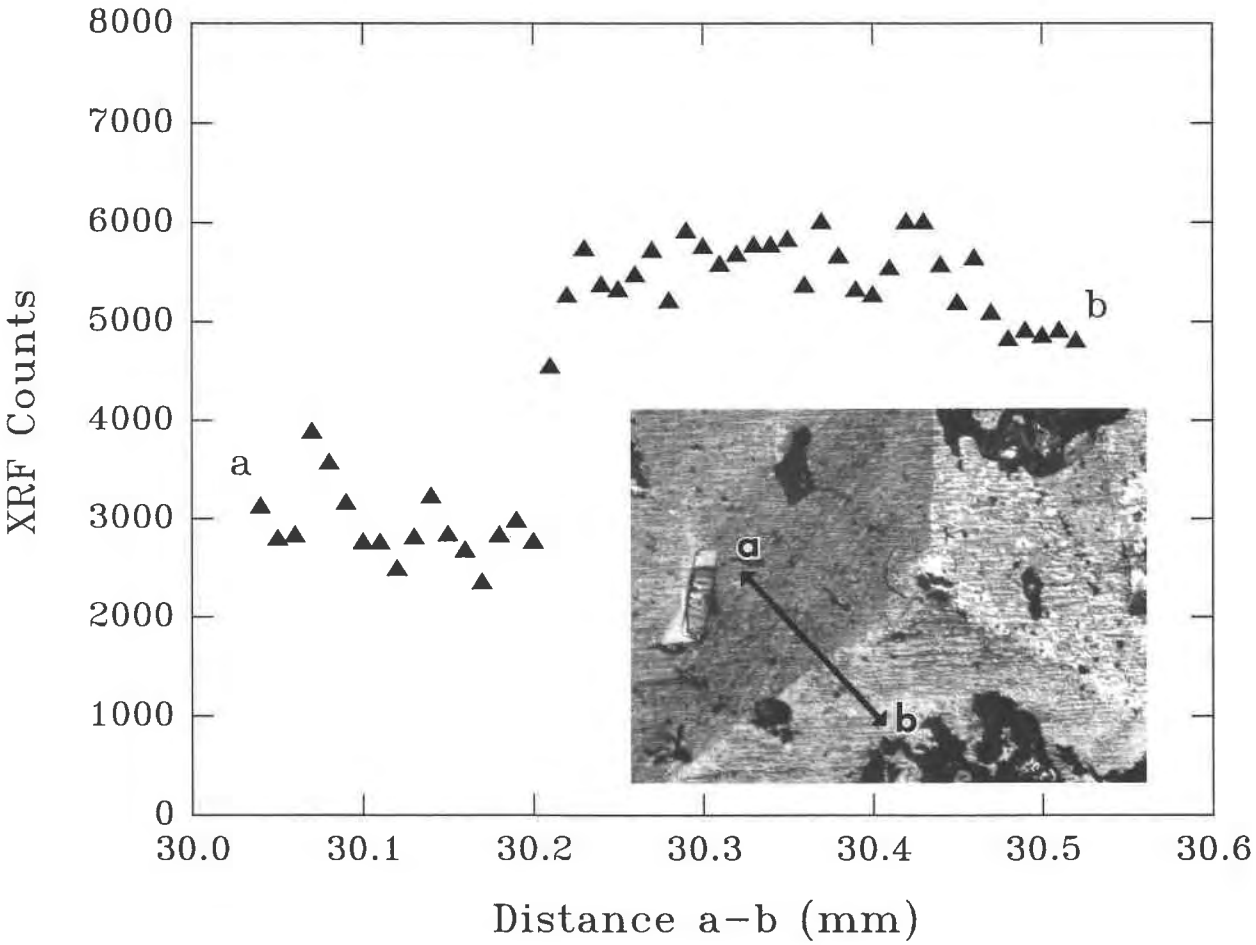

Fig. 9. The Y counts plotted for a SXRFMA line scan a-b between two nonequivalent vicinal faces of a $\{10\bar{1}0\}$ trigonal hillock on Golconda apatite no. 602a-2. A DIC photomicrograph of the hillock is inset. The sharp twofold increase in Y at 30.22 mm corresponds directly to the boundary between the two vicinal faces. Y concentrations at end points a and b are given in Table 1.

in CL are sharply delineated at the intersection of nonequivalent vicinal faces, suggesting that the compositional differences are discontinuous rather than gradational.

Compositional differences

SXRFMA point analyses (Table 1) and line (Fig. 9) and area scans (Fig. 10) also show that trace element differences correspond directly with subsectors of symmetrically nonequivalent vicinal faces of growth hillocks. In the $\{10\bar{1}0\}$ sectors, the concentration of Y is always higher, approximately by a factor of 2, in subsectors corresponding to the basal vicinal face of trigonal growth hillocks relative to those of the two symmetrically equivalent vicinal faces. As dictated by face symmetry, subsectors corresponding to the two equivalent vicinal faces do not show differences in Y concentration or in any other trace element. The absolute concentration of Y in the Golconda apatites varies from 200 ppm in the basal vicinal face and subsector to approximately 100 ppm in the symmetrically equivalent subsectors. Sr is also found to be preferentially incorporated, by a factor of 1.5–2, into the basal vicinal face subsector. The Sr concentration varies from 360 to 560 ppm. Because of the limited resolution available with EDS, it was not possible to determine quantitative differences in other trace elements (e.g., REE and Mn). However, there is qualitative evidence showing distributions of REE similar to that for Y. Cathodoluminescence also qualitatively suggests a differential distribution of REE. The absolute concentration of any individual REE or Mn atom is approximately 10–100 ppm. The minimum detection limit for these elements is approximately 1 ppm, using SXRFMA. Hence, trace elements found here produce signals that are substantially more intense than background.

Crystal growth

Incorporation of a trace element into a growing crystal is preceded by a series of phenomena, including transport to the surface, adsorption onto the surface, and possible surface diffusion to protosites (sites of incorporation). In the case of polyhedral crystals, which are bound by flat faces, growth occurs primarily by the spiral mechanism

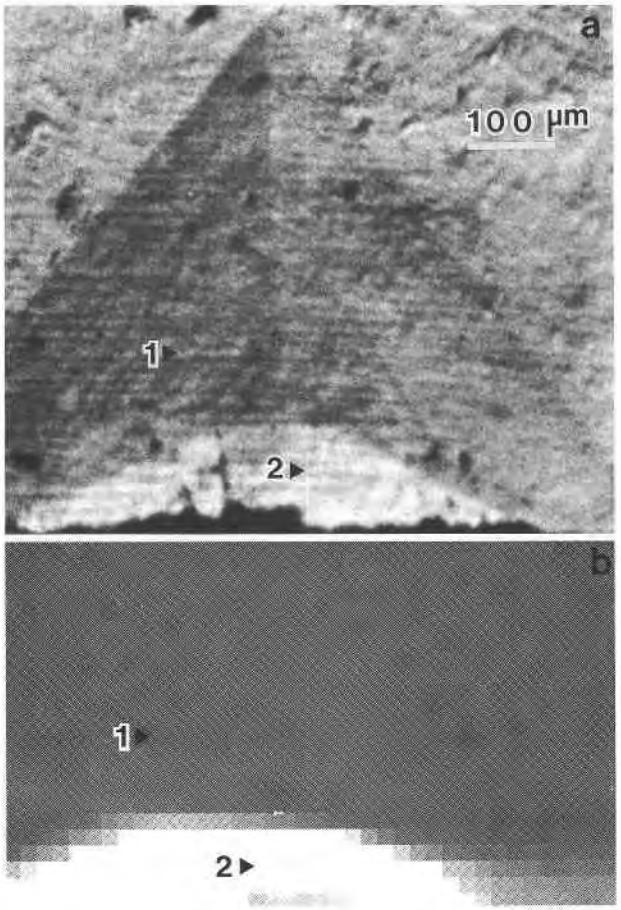

Fig. 10. (**a**) DIC photomicrograph of {10$\bar{1}$0} hillock on Golconda apatite no. 602c-1. Points 1 and 2 are identical in **a** and **b**. The nonequivalent vicinal face is the lightest region of the hillock, labeled 2. (**b**) Plot of Y concentration for SXRFMA area scan over the hillock in **a**. Absolute concentrations for points 1 and 2 are given in Table 1. High concentrations are plotted in lighter shades, and lower concentrations in gradationally darker shades. There is a direct correlation between the nonequivalent vicinal face and the high Y concentration, whereas the concentrations in the equivalent vicinal faces are the same.

(Sunagawa, 1987). Incorporation of growth units, and presumably of trace elements as well, takes place preferentially at kink sites along steps that have formed by the emergence of a screw dislocation at the surface of the crystal. Lateral advancement of a step occurs by repeated formation and filling of such kink sites. Compositional differences between time-equivalent portions of nonequivalent subsectors (intrasectoral zoning) form by growth at symmetrically different growth steps and vicinal faces. Because these compositional differences arise at the time of incorporation in the growth process, intrasectoral zoning indicates a differential affinity of symmetrically nonequivalent steps on a crystal surface for a particular trace element or possibly a paired substitution. Previous studies of intrasectoral zoning in calcite interpreted such differential partitioning to result from structural differences between nonequivalent growth steps of vicinal faces on growth hillocks (Paquette and Reeder, 1990; Staudt et al., 1994). Similarly, we propose that it is the geometry and coordination of available protosites within such growth steps that lead to the different affinities for a given element in different steps. Hence, the differential partitioning resulting in intrasectoral zoning in apatite is due to surface structural differences on growth steps of symmetrically nonequivalent vicinal faces.

Crystal faces and face symmetry

As a first approximation, a crystal face may be viewed as a truncation of a three-dimensional crystal structure along an energetically favorable plane. Dowty (1976a) interpreted this energetically favorable plane as a surface of least bonding: the surface that parallels a face over which the summation of potential bond energy is minimized. The arrangement of atoms within a slice along that plane, negating reconstruction and relaxation, is consistent with the plane symmetry of that face, a subset of the point group symmetry. Surfaces truncating the crystal structure that are not symmetrically related by the point group symmetry have different arrangements of atoms.

Kinetic factors may also influence the development and microtopography of crystal faces. Growth of an atomically flat crystal face is energetically less favorable than growth of a face exhibiting a microtopography. Many studies have shown that most crystal faces are not flat but exhibit a distinct surface microtopography. On morphologically important crystal faces (F and S forms: Hartman and Perdok, 1955), the microtopography is composed of growth steps. Most often steps are parallel to uninterrupted chains of strong bonds, so-called periodic bond chains (PBC) (Hartman and Perdok, 1955), in the crystal structure. In an analysis of the apatite structure, Terpstra et al. (1986) identified nine PBCs: ⟨0001⟩, ⟨10$\bar{1}$0⟩, ⟨10$\bar{1}$1⟩, ⟨1$\bar{1}$00⟩, ⟨12$\bar{3}$0⟩, ⟨12$\bar{3}$1⟩, ⟨12$\bar{3}$2⟩, ⟨$\bar{1}$2$\bar{1}$0⟩, and ⟨$\bar{2}$110⟩. There are three PBCs contained in a {10$\bar{1}$0} slice (a monolayer of thickness, d_{hkl}, deposited on a given face during layer growth): ⟨0001⟩, ⟨10$\bar{1}$0⟩, and ⟨10$\bar{1}$1⟩. The growth steps of the basal vicinal face on trigonal hillocks are parallel to ⟨0001⟩, and macrostep orientations on the other vicinal faces are roughly parallel to ⟨10$\bar{1}$1⟩. Growth steps on F faces are most often created by the intersection of a screw dislocation with the crystal face. Incorporation occurs preferentially at kink sites along these steps; consequently, it is more appropriate to view the growth surface as three-dimensional, with growth slices of finite thickness. Growth steps are commonly assumed to have a thickness equal to a slice (d_{hkl}) or some small multiple thereof (Dowty, 1976b). On an unrelaxed and unreconstructed surface, surface and step structure conform to face symmetry. On F forms, growth steps may have different orientations, and steps not related by face symmetry will have different atomic arrangements. In general, a given atomic site or polyhedron in the bulk

structure will also have a different surface representation or geometry where it appears in symmetrically nonequivalent steps.

The $\{10\bar{1}0\}$ in apatite is an F form. Intrasectoral zoning in the $\{10\bar{1}0\}$ sectors correlates with symmetrically different growth steps. Hence protosites in nonequivalent steps are expected to be structurally different. The results of modeling structural differences of these steps will be presented in another paper.

The role of growth rate on impurity incorporation

It has been shown (Burton et al., 1953) that there may be a strong correlation between the growth rate of a crystal and the effective partitioning behavior of an impurity or trace element. Hence, different faces of a crystal advancing at different rates may be expected to have different effective values of K_D, thereby leading to sectoral zoning. The model of Burton et al. (1953) assumes that diffusion of an impurity in the fluid in the vicinity of the advancing interface is the limiting factor controlling its incorporation. In this case, only the relative rates of normal advance of different faces are considered. It has not been shown, however, that the rate of growth will affect the observed value of K_D if a surface reaction is the rate limiting step in incorporation. Nevertheless, it is conceivable that if different growth steps on a given crystal face advance laterally at different rates, it could cause differential incorporation between those steps (cf. Trainor and Bartlett, 1961).

The morphology of a polygonized growth hillock is determined by the lateral rates of advance of the different growth steps it comprises. If one assumes equivalent step height on all vicinal faces, a hillock shows equal development of all vicinal faces only when their respective growth steps advance at the same rate. In all the apatite samples studied, there is approximately equal (symmetric) development of all vicinal faces on each hillock (Figs. 2 and 3). This equivalence indicates that lateral rates of advance of different growth steps are essentially the same. Therefore, the differential incorporation apparently cannot be attributed to differences in the rate of lateral advance of steps.

Asymmetrically developed trigonal growth hillocks on apatite from many other locations show generally equal development of the two symmetrically equivalent vicinal faces, as dictated by symmetry. In these samples, the basal vicinal face of trigonal growth hillocks is usually less well developed than the two equivalent vicinal faces, indicating that their lateral rates of advance are also controlled by step structure. Therefore, compositional variations that might correlate with different rates of step advance are ultimately due to different step structures.

Petrologic significance

To our knowledge, this is the first observation of intrasectoral zoning in a phosphate mineral. Moreover, the apatite samples that exhibit intrasectoral zoning are from several different locations. The presence of intrasectoral zoning in the samples studied as well as in several other apatite samples not described here suggests that this zoning type may be common in apatite. All the apatites studied were formed from hydrothermal solutions. However, intrasectoral and sectoral zoning are dependent on growth mechanism and may be found in other petrogenetic environments.

Researchers interested in the trace element chemistry of apatite may need to consider the implications of intrasectoral zoning in their studies. The presence of sectoral and intrasectoral zoning in apatite demonstrates a nonequilibrium distribution of trace elements between the fluid and crystal and further indicates that factors such as growth mechanism and surface structure are important in partitioning. However, intrasectoral zoning may go undetected by petrologists, given the small sizes of apatite crystals in igneous rocks and the spatial resolution of analytical techniques commonly used today. In some cases, compositional measurements are made on multiple crystals, and intracrystalline heterogeneities are thus missed altogether and averaged. However, as techniques with better spatial resolution and higher sensitivity, such as SXRFMA and ion microprobe, become more widespread, common sectoral and intrasectoral zoning may be revealed. SXRFMA also allows in-situ analysis of individual crystals within whole-rock samples rather than mineral separates.

Even if such zoning was detected, the magnitude of compositional variation in some apatite samples may be insignificant for the petrologist modeling igneous processes. However, in the case of apatite containing very large amounts of REE (as much as a few weight percent), variations of a factor of 2–3 may be quite significant for mass balance calculations and for modeling of elemental distribution in magmatic systems.

The systematics of sectoral and intrasectoral zoning should be very significant to the petrologist or geochemist trying to understand the nature of trace element partitioning and the factors affecting it. Geochemists often use partition coefficients, K_D, to define the affinity of a particular mineral for a given element relative to the fluid from which it formed. Several studies have experimentally determined partition coefficients for trace elements in apatite, such as Sr, Mn, and REE (Kovalenko et al., 1982; Watson and Green, 1981). The surface structural controls on partitioning seen in apatite not only exemplify that mechanistic factors play a role in partitioning but also demonstrate that empirically determined values of K_D for a given mineral-fluid system are not unique; rather, effective K_D values differ for structurally distinct regions of a crystal surface. Furthermore, the empirically determined bulk K_D value of a mineral is an average of the values associated with each individual sector and subsector in the crystal. It is dependent not only on growth mechanism but also on the relative volume of each type of sector and subsector present (i.e., crystal habit).

The combination of concentric, sectoral, and intrasectoral zoning can obviously lead to very complex zoning patterns that may be misinterpreted in randomly oriented sections. Several authors (Marshall, 1988; Jolliff et al., 1989) have noted a clustering or patchy distribution of REE within individual crystals of apatite. Several explanations have been given, but it is quite possible that such anomalous distributions are due to intrasectoral or sectoral zoning.

Optical anomalies

Llallagua apatite samples not only exhibit sectoral and intrasectoral zoning but also show optically anomalous regions that correspond directly with different sectors and subsectors. Ordering of REE, Mn, and Sr has been shown to occur between the Ca1 and Ca2 sites without lowering the symmetry from $P6_3/m$ (Hughes et al., 1991a, 1991b). Substitution of Si for $^{[4]}$P, which may occur in these samples, could lead to ordering that would lower the symmetry (Hughes and Drexler, 1991). However, the anomalous optical behavior may not be due to compositional differences because the degree of compositional variation found among these samples is also present in other apatites that are entirely uniaxial negative. Therefore, the cause of the symmetry reduction may be the ordering of column anions: either F,OH ordering or OH directional ordering. The direct correlation of optical character with different sectors and subsectors indicates that surface structure also plays a role in the ordering of trace or major elements in these apatite samples during growth.

Dissymmetrization, or the lowering of the symmetry of a crystal, has been noted in many minerals, including grossular, chabazite, topaz, leucite, and analcime. In most cases, optically anomalous behavior associated with dissymmetrization is due to the ordering of atoms in the crystal. Gali (1983) proposed that ordering of Fe and Al in octahedral sites of grossular-andradite garnets could occur during growth, and that ordering was controlled by the surface structure of growth steps on {110} faces. This idea of ordering controlled by surface structure during growth was first proposed by Akizuki and Sunagawa (1978) and is one possible explanation for optically anomalous behavior in other minerals (e.g., Akizuki et al., 1979; Akizuki, 1981). Neutron diffraction experiments should allow one to determine structure and ordering in the individual sectors and subsectors of the Llallagua apatite specimens.

Acknowledgments

We thank Anthony Kampf of the Los Angeles Museum of Natural History for providing the Llallagua apatite samples (LAMNH no. 35673), George Harlow of the American Museum of Natural History for the Llallagua-2 apatite (AMNH no. 32870), and Neil Pfaff for the Golconda apatite samples. Our deepest gratitude is extended to Mark Rivers and Steve Sutton for their unending help at the National Synchrotron Light Source. We also thank John M. Hughes and R. Chris Tacker for their helpful reviews. This study was supported by NSF grant EAR-9204809.

References cited

Akizuki, M. (1981) Origin of optical variation in analcime. American Mineralogist, 66, 403–409.

Akizuki, M., and Sunagawa, I. (1978) Study of the sector structure in adularia by means of optical microscopy, infra-red absorption, and electron microscopy. Mineralogical Magazine, 42, 453–462.

Akizuki, M., Hampar, M.S., and Zussman, J. (1979) An explanation of anomalous optical properties of topaz. Mineralogical Magazine, 43, 237–241.

Bergman, S.C. (1979) The significance of accessory apatite in the REE modelling of magma genesis. Eos, 60, 412.

Burns, R.G. (1970) Mineralogical applications of crystal field theory, p. 144–174. Cambridge University Press, Cambridge, U.K.

Burton, J.A., Prim, R.C., and Slichter, W.P. (1953) The distribution of solute in crystals grown from the melt. I. Theoretical. Journal of Chemical Physics, 21, 1987–1991.

Criss, J.W. (1977) NRLXRF: A Fortran program for x-ray fluorescence analysis. Naval Research Laboratory, Washington, DC.

Dowty, E. (1976a) Crystal structure and crystal growth. I. The influence of internal structure of morphology. American Mineralogist, 61, 448–459.

——— (1976b) Crystal structure and crystal growth. II. Sector zoning in minerals. American Mineralogist, 61, 460–469.

——— (1977) The importance of adsorption in igneous partitioning of trace elements. Geochimica et Cosmochimica Acta, 41, 1643–1646.

Gali, S. (1983) Grandite garnet structures in connection with growth mechanism. Zeitschrift für Kristallographie, 163, 43–52.

Goldschmidt, V.M. (1937) The principles of distribution of chemical elements in minerals and rocks. Journal of the Chemical Society of London, 655–673.

Gromet, L.P., and Silver, L.T. (1983) Rare earth element distributions among minerals in a granodiorite and their petrologic implications. Geochimica et Cosmochimica Acta, 47, 925–938.

Hartman, P., and Perdok, W.G. (1955) On the relations between structure and morphology of crystals. I. Acta Crystallographica, 8, 49–52.

Hughes, J.M., and Drexler, J.W. (1991) Cation substitution in the apatite tetrahedral site: Crystal structures of type hydroxylellestadite and type fermorite. Neues Jahrbuch für Mineralogie Monatshefte, H7, 327–336.

Hughes, J.M., Cameron, M., and Crowley, K.D. (1989) Structure variations in natural F, OH and Cl apatites. American Mineralogist, 74, 870–876.

——— (1990) Crystal structures of natural ternary apatites: Solid solution in the $Ca_5(PO_4)_3X$ (X = F, OH, Cl) system. American Mineralogist, 75, 295–304.

——— (1991a) Ordering of divalent cations in the apatite structure: Crystal structure refinements of natural Mn- and Sr-bearing apatite. American Mineralogist, 76, 1857–1862.

Hughes, J.M., Cameron, M., and Mariano, A.N. (1991b) Rare-earth-element ordering and structural variations in natural rare-earth-bearing apatites. American Mineralogist, 76, 1165–1173.

Jolliff, B.L., Papike, J.J., and Shearer, C.K. (1989) Inter- and intra-crystal REE variations in apatite from the Bob Ingersoll pegmatite, Black Hills, South Dakota. Geochimica et Cosmochimica Acta, 53, 429–441.

Jones, K.W., and Gordon, B.M. (1989) Trace element determinations with synchrotron-induced X-ray emission. Analytical Chemistry, 61, 341A.

Kampf, A.R. (1982) Jeanbandyite a new member of the Stottite group from Llallagua, Bolivia. Mineralogical Record, 13, 235–239.

Kovalenko, V.I., Antipin, V.S., Vladykin, N.V., Smirnova, Y.V., and Balashov, Y.A. (1982) Rare-earth distribution coefficients in apatite and behavior in magmatic processes. Geokhimiya, 2, 230–242.

Marshall, D.J. (1988) Cathodoluminescence of geologic materials, p. 47–123. Unwin Hyman, Winchester, Massachusetts.

McConnell, D. (1973) Apatite: Its crystal chemistry, mineralogy, utilization and geologic and biologic occurrences, p. 22–31. Springer-Verlag, New York.

Nakamura, Y. (1973) Origin of sector zoning in igneous clinopyroxenes. American Mineralogist, 58, 986–990.

Nash, W.P. (1972) Apatite chemistry and phosphorus fugacity in a differentiated igneous intrusion. American Mineralogist, 57, 877–886.

Paquette, J., and Reeder, R.J. (1990) A new type of compositional zoning in calcite: Insights into crystal-growth mechanisms. Geology, 18, 1244–1247.

Proctor, K. (1985) Gem pegmatites of Minas Gerais Brazil: The tourmalines of the Governador Valadares District. Gems and Gemology 21, 86–104.

Rakovan, J., and Reeder, R.J. (1992) Differential distribution of REE and Mn in apatite as controlled by crystal surface structure. Geological Society of America Meeting Abstracts with Program, 24, A175.

——— (1993) Differential ordering and trace element incorporation in apatite: The role of surface structure during growth. Spring American Geophysical Union Meeting Abstracts, with Program, 74, 342.

Reeder, R.J., and Grams, J.C. (1987) Sector zoning in calcite cement crystals: Implications for trace element distributions in carbonates. Geochimica et Cosmochimica Acta, 51, 187–194.

Ringwood, A.E. (1955) The principles governing trace element distribution during crystallization. I. The influence of electronegativity. Geochimica et Cosmochimica Acta, 7, 189–202.

Ronsbo, J.G. (1989) Coupled substitutions involving REEs and Na and Si in apatites in alkaline rocks from the Ilímaussaq intrusion, South Greenland, and the petrological implications. American Mineralogist, 74, 896–901.

Staudt, W.J., Reeder, R.J., and Schoonen, M.A.A. (1994) Surface structural controls on compositional zoning of SO_4^{2-} and SeO_4^{2-} in synthetic calcite single crystals. Geochimica et Cosmochimica Acta, 58, 2087–2098.

Stormer, J.C., Jr., Pierson, M.L., and Tacker, R.C. (1993) Variation of F and Cl X-ray intensity due to anisotropic diffusion in apatite during electron microprobe analysis. American Mineralogist, 78, 641–648.

Sunagawa, I. (1987) Morphology of minerals. In I. Sunagawa, Ed., Morphology of crystals, p. 509–587. Terre Scientific, Tokyo.

Terpstra, R.A., Bennema, P., Hartman, P., Woensdregt, C.F., Perdok, W.G., and Senechal, M.L. (1986) F faces of apatite and its morphology: Theory and observation. Journal of Crystal Growth, 78, 468–478.

Trainor, A., and Bartlett, B.E. (1961) A possible mechanism of crystal growth from the melt and its application to the problem of anomalous segregation at crystal facets. Solid-State Electronics, 2, 106–114.

Watson, E.B., and Capobianco, C.J. (1981) Phosphorus and rare-earth elements in felsic magmas: An assessment of the role of apatite. Geochimica et Cosmochimica Acta, 45, 2349–2358.

Watson, E.B., and Green, T.H. (1981) Apatite/liquid partition coefficients for the rare earth elements and strontium. Earth and Planetary Science Letters, 56, 405–421.

Watson, E.B., and Harrison, T.M. (1984a) Accessory minerals and the geochemical evolution of crustal magmatic systems: A summary and prospectus of experimental approaches. Physics of the Earth and Planetary Interiors, 35, 19–30.

——— (1984b) What can accessory minerals tell us about felsic magma evolution? A framework for experimental study. Proceedings of the 27th International Geologic Congress, 11, 503–520.

Manuscript received September 24, 1993
Manuscript accepted April 29, 1994